EUMETSAT ECMWF

EUMETSAT/ECMWF Fellowship Programme
Research Report

53

Reducing the drying effect through a water vapour correction to the all-sky error model

Katrin Lonitz and Alan J. Geer

May 2020

Series: EUMETSAT/ECMWF Fellowship Programme Research Reports

A full list of ECMWF Publications can be found on our website under:
http://www.ecmwf.int/en/research/publications

Contact: library@ecmwf.int

European Centre for Medium-Range Weather Forecasts, Shinfield Park, Reading, RG2 9AX, UK

Abstract

In the past the assimilation of microwave imagers caused a small drying around 850 hPa, additional to a dry model climate. The additional drying effect has mostly been reduced due to the activation of 150/166 GHz channels at IFS cycle 46R1, and to a lesser extent due to changes in the humidity background error formulation at IFS cycle 43R3. This report investigates whether specific aspects of the observation error model can explain the remaining drying effect. First, using bias corrected values to compute the symmetric cloud amount $\overline{C37}$ barely affect the observation error model. Second, the drying mainly occurs in almost cloud-free scenes, which led to a further hypothesis that the representation of water vapour in the observation error model in these cases could be related to the dry bias. Using reconstructed values for clear sky brightness temperatures at 37 GHz as part of the observation error model allowed a more symmetric treatment of how water vapour affects the clear sky polarisation difference at 37 GHz ($P37^{clr}$) for observations and first guess. Combining both updates in the computation of $\overline{C37}$ delivers the largest reduction in the additional drying effect associated with almost cloud-free conditions. However, the overall effect of these modifications of the observation error model is quite small, as seen in the neutral impact on forecast scores and neutral fits to independent observations. Having in mind the technical work required, we do not recommend the modifications in the computation of symmetric cloud amount for an operational model.

1 Background

Since 2009 microwave imager (MWI) radiances have been assimilated operationally in clear, cloudy and precipitating (also known as all-sky) conditions into the ECMWF numerical weather prediction system [Bauer et al., 2010, Geer et al., 2010]. Despite improvements in forecast scores through all-sky assimilation [Geer et al., 2017] an unwanted side effect has been a drying of the analysis. This can be seen in the analysis values of total column water vapour when comparing 41R1 simulations in which MWI data is assimilated actively (**active all-sky**) and passively[1] (**passive all-sky**). To avoid any interaction or compensation effects between imager and sounder channels the assimilation of the sounding channels from Special Sensor Microwave Imager/Sounder onboard of DMSP-F17 and DSMP-F18 (SSMIS-F17/F18) and GPM Microwave Imager (GMI) is also omitted in these experiments. In Fig. 1 large patches of mean drying of around 1 kg m^{-2} can be seen over most parts of the tropical oceans. But comparing quantitative measures of water vapour comes with its pitfalls, as the largest changes can often be seen in regions with the largest amount of water vapour - the Tropics. Hence, it is good to check how a relative measure of water vapour changes, e.g. relative humidity.

To focus on the lower troposphere where most of the water vapour is located we have chosen to study relative humidity at 850 hPa. When comparing the **active all-sky** and the **passive all-sky** as done in Fig. 2, large patches of mean drying of around 2% to 6% over most parts of the oceans have been detected when MWI data is actively assimilated. Only in the Pacific along the West coast of North America and northern South America, as well as along the East coast of Asia areas of moistening are prevalent. This is partly related to a model bias in stratocumulus regions [Lonitz and Geer, 2017]. Overall, the addition of microwave imager data caused a relative reduction in relative humidity of about 10% and a relative increase in temperature of about 3% in the analysis, averaged over areas where MWI data is prevalent i.e. over ocean between 60°S and 60°N.

Nevertheless, an excessive dryness of the analysis is not only the result of the assimilation of microwave imagers since it is also present without them. Fits to radiosonde humidity observations in Fig. 3 show that even without the assimilation of microwave imagers, the analysis is too dry compared to the radiosonde

[1] Passive assimilation means that data does not affect the analysed atmospheric state and only the bias correction is adapted to fit the relevant observations.

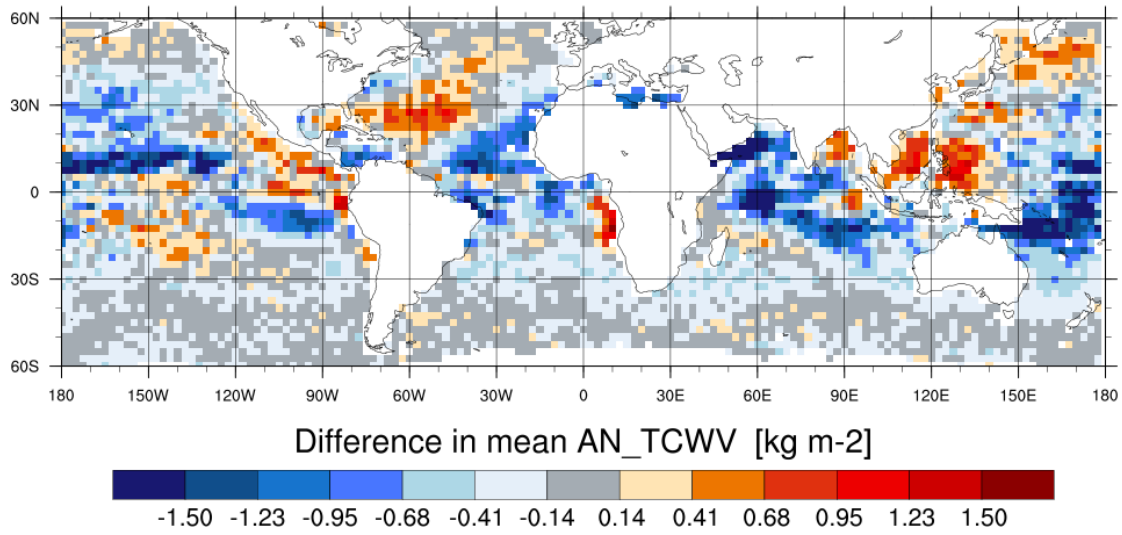

Figure 1: Difference in time-mean analysis total column water vapour (TCWV) between a cycle 41R1 experiment with actively assimilated SSMIS data (**active all-sky**) and a cycle 41R1 experiment with passively assimilated SSMIS data (**passive all-sky**). Additionally, both experiments exclude the assimilation of SSMIS sounding channels. Blue colours correspond to a reduction (drying) and red colours correspond to an increase (moistening) in TCWV for the **active all-sky** experiment. Data has been accumulated in observation space at SSMIS location. Means have been computed over the time period 11 June to 31 July 2014 and in bins of 2.5°lat $\times$ 2.5°lon bin, with bins having less than 50 samples being excluded.

observations. The drying is largest at 850 hPa with analysis departures of about 5.2×10^{-5} kg kg^{-1} for passive all-sky and about 6.0×10^{-5} kg kg^{-1} for active all-sky in IFS cycle 45R1. Hence, only about 13% of the bias compared to radiosonde can be attributed to the assimilation of radiances from microwave imagers. The mean bias is, additionally, not all down to the assimilation of satellite observations. This can be seen in the green line in Fig. 3 where no satellite radiances from microwave imagers or sounders in clear or all-sky conditions have been assimilated and atmospheric motion vectors, clear-sky radiances from various geostationary platforms, hyperspectral infrared radiances and GPSRO data have also been removed. The fit to radiosonde observations shows a mean bias of about 4×10^{-5} kg kg^{-1} in the lower atmosphere even before satellite observations are assimilated. The model climate is most likely drier to that of the radiosondes.

The additional drying effect caused by the assimilation of microwave imagers could have many reasons. For example, the interplay between model bias and variational bias correction might contribute to the drying, as discussed by Eyre [2016]. One of his findings was that the effect of model bias on analysis biases increases with more observations being bias-corrected. In other words, the additional drying seen through the assimilation of bias-corrected radiances from microwave imagers could be caused by the dry model bias and even amplified when more microwave imagers are being assimilated. Another reason is based in the observation and background error formulations for humidity, as this led to an unbalanced system in preferring dry conditions over humid ones. This imbalance was partly corrected when the humidity background error model was updated in IFS cycle 43R3, in which these errors have in general increased [Buizza et al., 2017].

In this study, we focus if changes to the observation error model can explain the remaining additional

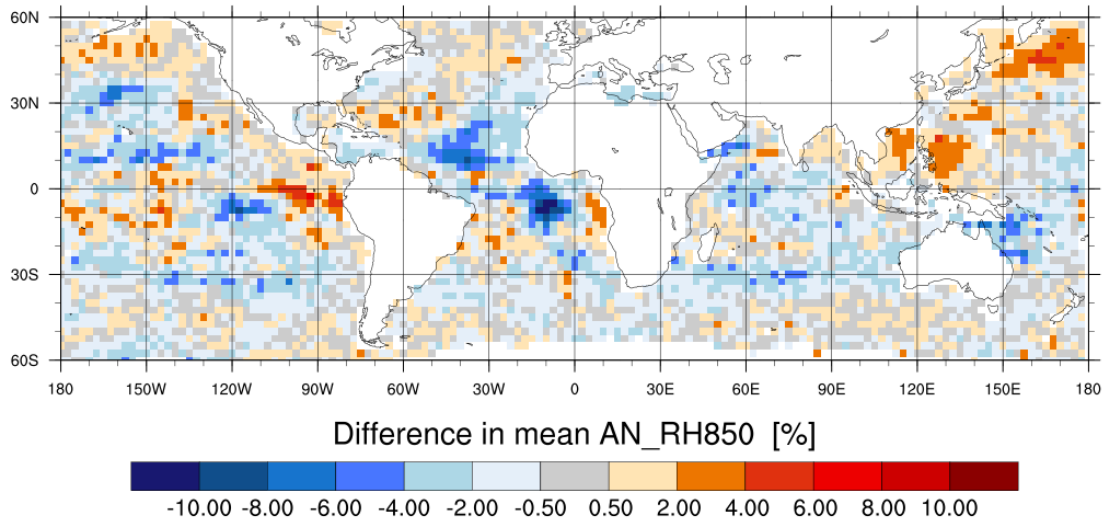

Figure 2: Difference in time-mean analysis humidity at 850 hPa between a cycle 41R1 experiment with actively assimilated SSMIS data (**active all-sky**) and a cycle 41R1 experiment with passively assimilated SSMIS data (**passive all-sky**). Additionally, both experiments exclude the assimilation of SSMIS sounding channels. Blue colours correspond to a reduction (drying) and red colours correspond to an increase (moistening) in relative humidity for the **active all-sky** experiment. Data has been accumulated in observation space at SSMIS location. Means have been computed over the time period 11 June to 31 July 2014 and in bins of 2.5°lat × 2.5°lon bin, with bins having less than 50 samples being excluded.

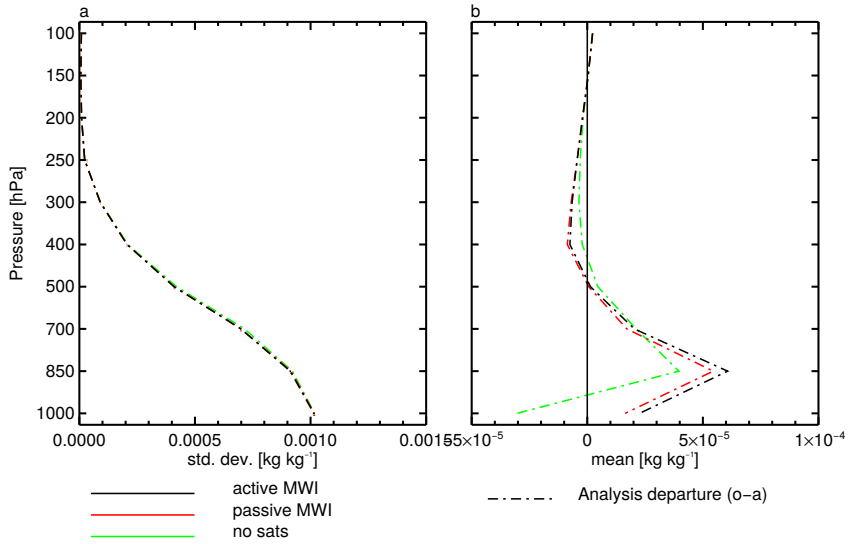

Figure 3: Vertical profile of a) standard deviation and b) mean values in analysis departures for radiosonde specific humidity observations of cycle 45R1 experiments with (**active all-sky**; black) and without (**passive all-sky**; red) the assimilation of MWI, and no assimilation of most satellite radiances or products (no sats: no assimilation of microwave imagers and sounders, of atmospheric motion vectors, of clear-sky radiances from various geostationary platforms, of hyperspectral infrared radiances and of GPSRO data; green). Results are shown for the time period between 11 June and 31 July 2017.

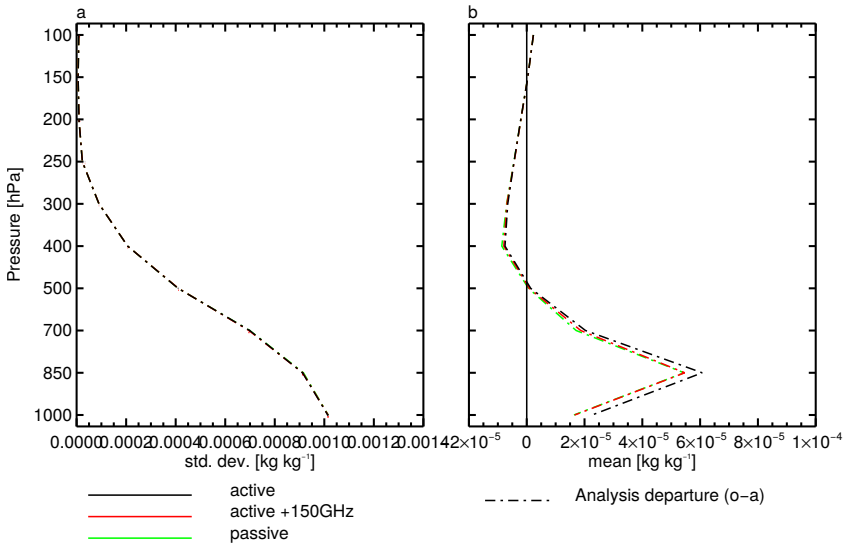

Figure 4: Vertical profile of a) standard deviation and b) mean values of analysis departures for radiosonde specific humidity observations from radiosonde of 45R1 experiments with (**active all-sky** [black]; **active all-sky** + 150 GHz [red]) and without (**passive all-sky** [green]) assimilating MWI. Results are shown for the time period between 11 June and 31 July 2017.

drying effect seen through the addition of microwave imager data. For this purpose we study experiments using IFS cycle 45R1. Compared to results seen in Fig. 2 for IFS cycle 41R1 in 2014, the most relevant change is the increase in the amount of microwave radiances in all-sky conditions, which does influence the additional drying effect of microwave imager radiances. For example, more microwave imagers (GMI and AMSR2) and more microwave sounders (MWHS-2, MHS, SAPHIR) are assimilated under all-sky conditions than in 2015. Furthermore, the addition of new channels around 150 GHz from SSMIS-F17 and GMI (activated in IFS cycle 46R1) reduces the additional drying effect further, as seen in Fig. 4. Here, the addition of the 150/166 GHz channels reduces the dry bias at 850 hPa from about 6.0×10^{-5} kg kg^{-1} to 5.5×10^{-5} kg kg^{-1} for **active all-sky** similar to the **passive all-sky**. This reduction in the additional drying effect occurs mostly outside the tropics (areas south of 20°S and north of 20°N; not shown).

Fig. 5 shows the difference in relative humidity at 850 hPa between an **active all-sky** and a **passive all-sky** experiment using IFS cycle 45R1. The addition of 150/166 GHz in Fig. 5b compared to Fig. 5a reduces the drying in some areas and increases the moistening in others, but to a small extent. The global mean difference in humidity for Fig. 5b is close to zero. The remaining large biases are now restricted to the positive biases in stratocumulus regions, and some biases in the NH higher latitudes. Those biases are associated with cloudy conditions (see Fig. 6), whereas for almost cloud-free conditions (cloud amount less than 5%) the additional drying effect is only reduced by roughly 50% through the addition of 150/166 GHz channels (see Tab. 1). The addition of these channels reduces the drying most likely because MWI observations contain column integrated information on humidity, cloud, rain, and information on the surface. Using this information to correctly adjust the analysis at every single height level can be challenging. The largest role in the vertical attribution of where the increments should be made is played by the background errors. Nevertheless, using additional information like the 150 GHz channels can help to improve on this issue by improving the vertical sensitivity in the lower atmosphere.

Even though the additional drying effect seen through the assimilation of microwave imagers has been

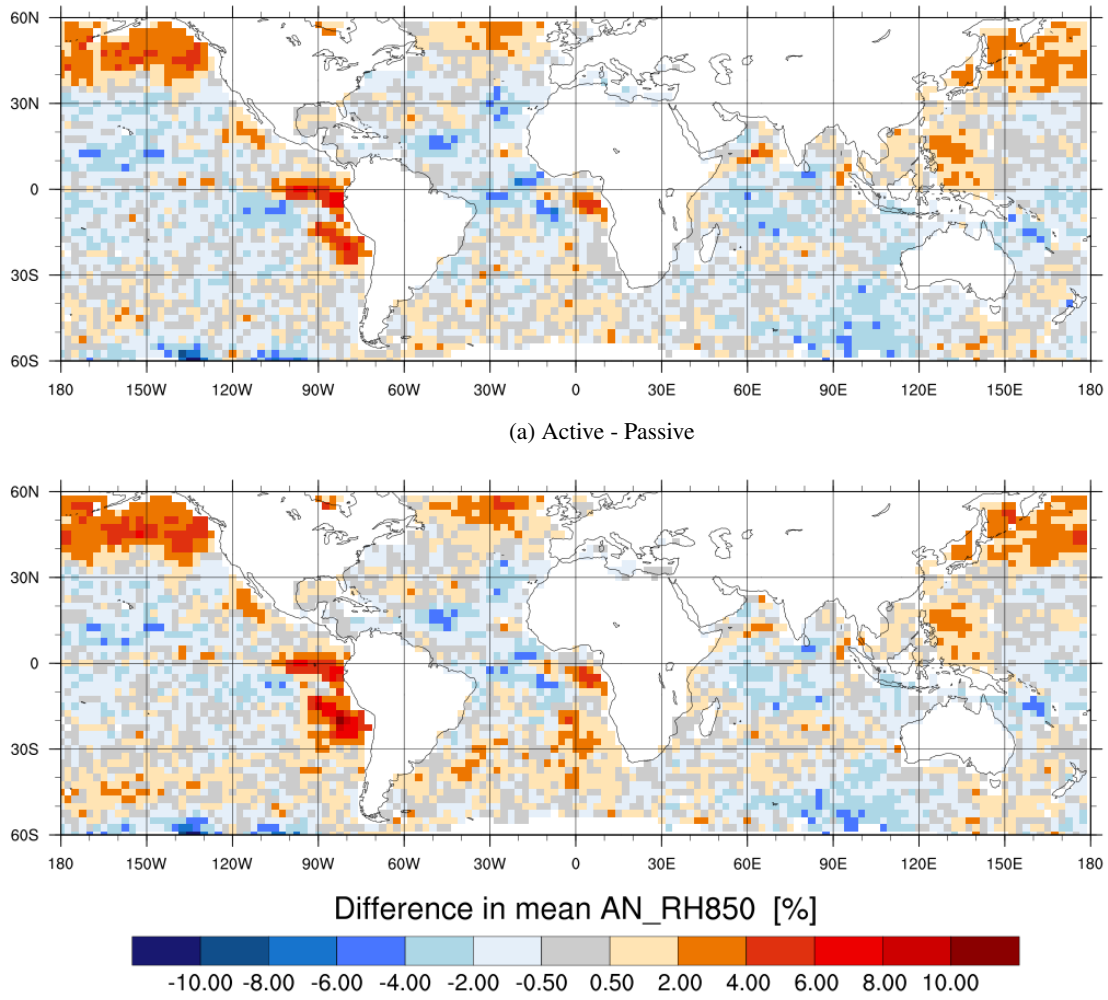

(a) Active - Passive

(b) Active + 150 GHz - Passive

Figure 5: As Fig. 2 just for 45R1 experiments. The means are taken over the time period 11 June to 31 July 2017.

Table 1: Mean analysis relative humidity [%] at 850 hPa for active all-sky experiments compared to passive all-sky experiment for low cloud amount ($\overline{C37}$, explained later in section 3) smaller than 5%. Mean and standard error are computed over the time period 11 June to 31 July 2017 at observation locations.

configuration	mean ± std. error	difference to **passive all-sky**
active all-sky	58.60 ± 0.18	-1.29 ± 0.04
active all-sky + 150/166 GHz	59.23 ± 0.18	-0.66 ± 0.04
passive all-sky	59.89 ± 0.18	

clearly decreased since IFS cycle 41R1 through the update of the humidity background error (IFS cycle 43R3) and the addition of 150/166 GHz channels (IFS cycle 46R1), there is still some drying effect seen for conditions with a small cloud amount. This study examines the hypothesis if an imbalance in the observation error model could cause such a drying. To create a dry bias the error would have to be smaller for observations contributing to a drying than for observations contributing to a moistening. For the all-sky assimilation the observation errors are assigned based on cloud amount, which is a simple retrieval using brightness temperatures at 37 GHz from the two different polarisations, vertical and horizontal. However, the retrieval depends on the background water vapour being accurate. Error in background water vapour can cause this simple cloud amount retrieval to be moderately erroneous, which would lead to observation errors being too large or too small. If the water vapour is underestimated the retrieved cloud amount would be overestimated, which translates into assigning too large observation errors. Our hypothesis is that these areas with underestimated water vapour content in almost cloud-free conditions play an important role in the additional drying effect because they are unable to moisten the atmosphere as much as they could compared to if their observation errors were smaller.

2 Data and setup

Different sets of experiments have been created (see Table 2) with a resolution of TCo399 using IFS cycle 45R1 from 1 June to 31 August 2017 and without the active assimilation of the sounding channels from Special Sensor Microwave Imager/Sounder onboard of DMSP-F17 and DSMP-F18 (SSMIS-F17/F18) and GPM Microwave Imager (GMI). The experiments are similar to the active all-sky and the passive all-sky experiments mentioned in section 1. The passive all-sky experiment does not assimilate any microwave imager data; i.e. the tangent linear and adjoint of the observation operator are set to zero except for the bias correction of this particular set of observations. The active all-sky experiments add only the assimilation of SSMIS-F17 (i.e. no assimilation of AMSR2 and GMI). Furthermore, different configurations of all-sky experiments are tested (as listed in Table 2). The **control** uses the default setup as described above and is designed to investigate why an additional drying occurs and how it is linked to an imbalance in the observation error model of the all-sky assimilation of microwave imager data (section 3). **Exp. 1** and **exp. 2** are modifications of **control** in order to reduce the imbalance in the observation error model, as described in sections 4 and 5, respectively. The **control** configuration is also used for the passive all-sky experiment (**no MWI**).

3 Relationship between the drying and cloud amount

The observation error model in all-sky data assimilation is related to the symmetric cloud amount, $\overline{\mathrm{C37}}$, which estimates how much cloud is on average in the first guess and the observations [Geer and Bauer, 2010]:

$$\overline{\mathrm{C37}} = \frac{\mathrm{C37}_{\mathrm{obs}} + \mathrm{C37}_{\mathrm{fg}}}{2}, \tag{1}$$

with the observed cloud amount, $\mathrm{C37}_{\mathrm{obs}}$, and the first guess cloud amount, $\mathrm{C37}_{\mathrm{fg}}$. Here, C37 is defined as:

$$\begin{aligned} \mathrm{C37} &= 1 - \mathrm{P37} \\ &= 1 - \frac{T_v - T_h}{{T_v}^{clr} - {T_h}^{clr}}, \end{aligned} \tag{2}$$

with P37 the normalised polarisation difference at 37 GHz, and T_v and T_h are the vertically and horizontally polarised 37 GHz brightness temperatures at the top of the atmosphere. Their cloud- and precipitation free counterparts are ${T_v}^{clr}$ and ${T_h}^{clr}$. Here, T_v - T_h is a measure of atmospheric opacity. If the atmosphere is very opaque (e.g. very cloudy or moist) T_v and T_h would be very similar. This is because the atmospheric absorption is in general unpolarised, whereas emission from the sea surface is highly polarised. Normalisation of T_v - T_h by its cloud- and precipitation free counterpart gives a measure that depends on the atmospheric transmittance due to cloudiness [see Eq. (4)]. Because ${T_v}^{clr}$ and ${T_h}^{clr}$ are only known for the first guess field they are used for both the computation of $\mathrm{C37}_{\mathrm{obs}}$ and $\mathrm{C37}_{\mathrm{fg}}$. This is how water vapour errors in the first guess can potentially introduce an error in the calculation of $\mathrm{C37}_{\mathrm{obs}}$, as discussed later.

Fig. 6 shows the spatial distribution of $\overline{\mathrm{C37}}$ for the **control**. Over most parts of the ocean the average value of $\overline{\mathrm{C37}}$ is small and less than 0.1. In convective regions (e.g. ITCZ) and the mid-latitude storm tracks (e.g. around 55°S) $\overline{\mathrm{C37}}$ can reach values up to 0.2 and more on average. It can be seen that areas of drying as highlighted in Fig. 5a are often associated with areas with small $\overline{\mathrm{C37}}$ values. Putting it differently, the dry bias can be seen for less cloudy areas.

To investigate the relationship between the drying of the analysis and $\overline{\mathrm{C37}}$ more quantitatively, the difference in instantaneous fields of the analysis relative humidity at 850 hPa between the active and passive all-sky experiment (**control** and **no MWI**) is plotted against $\overline{\mathrm{C37}}$ (Fig. 7). For $\overline{\mathrm{C37}}$ less than or equal to 0.1 the mean in relative humidity difference departs from zero and drops to negative values down to - 5%, i.e. the relative humidity is reduced in the active all-sky experiment compared to the passive all-sky experiment. However, it is interesting to see that the drying is only associated with cases which are clear or nearly clear. This suggests that the observation error model which depends directly on $\overline{\mathrm{C37}}$ plays an

Table 2: List of undertaken experiments.

configuration	**active all-sky**	**passive all-sky**
control	✓	
exp. 1: bias-corrected $\overline{\mathrm{C37}}$	✓	
exp. 2: bias-corrected $\overline{\mathrm{C37}}$ + reconstructed P37 ${}^{clr}_{rec}$	✓	
no MWI: as **control**		✓

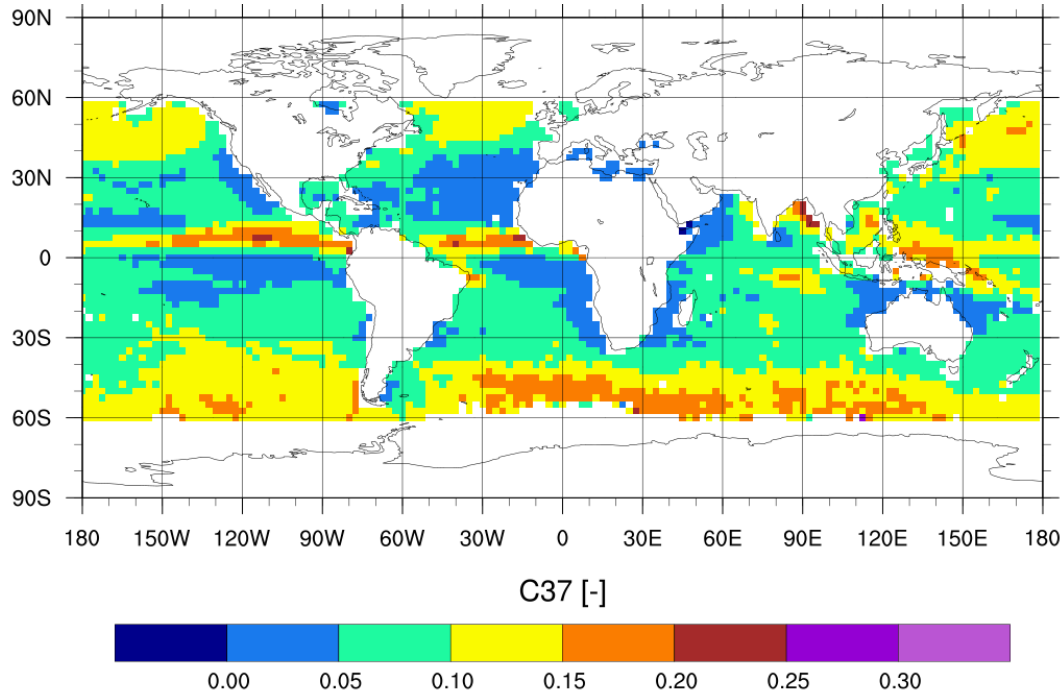

Figure 6: Mean symmetric cloud amount at observation location of SSMIS-F17 data from **control** experiment. The mean is taken for every 2.5°lat $\times$ 2.5°lon bin and over the time period 11 June to 31 July 2017.

important role in the drying. Roughly speaking the lower the mean cloudiness the smaller the observation error and hence, the larger the weight the observations have in the assimilation [for more details see Geer and Bauer, 2010]. In other words, the large difference in relative humidity in the active all-sky experiment compared to the passive one could be caused through the assimilation of observations which have a large weight (low cloud amount) and which seem to force the analysis towards drier conditions.

3.1 Trace of drying in increments

If the assimilation of microwave imager data is the reason why the analysis is dried it should be possible to detect the same feature as seen in Fig. 7, i.e. that the drying occurs for samples with low cloud amount, in the humidity increment for the active all-sky experiment, too. Here, the relative humidity increment (Fig. 8a), as well as the TCWV increment (Fig. 8b) are negative for $\overline{C37}$ smaller than 0.1, i.e. the humidity is reduced in the analysis compared to the first guess for samples with low cloud amount. The knowledge that the drying in the analysis can also be seen in the humidity increments and departures of the active all-sky experiment further suggests that the observation error model plays a role in the drying process.

3.2 Trace of drying in departures

In order to check why the drying seems to be linked to characteristics of the observation error model, Fig. 9 shows the observation error as a function of first guess departure. Here, the minimum of the observation error for SSMIS-F17 channel 16 (37 v GHz) is 1.8 K and increases with increasing symmetric cloud amount. As expected, the median observation error is larger for positive FG dep values with 3.4 K than

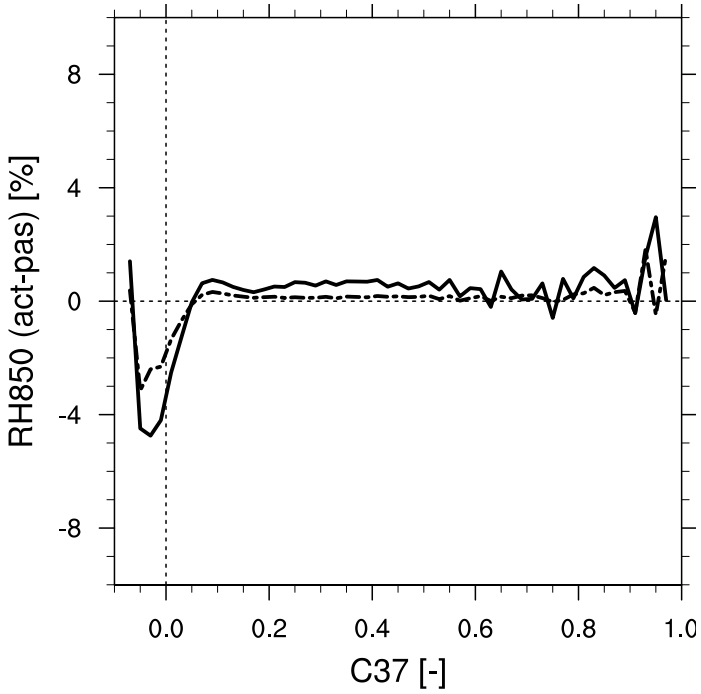

Figure 7: Binned mean (solid line) and median (dashed-dotted line) difference in analysis relative humidity at 850 hPa between the active and passive 45R1 all-sky experiment as a function of $\overline{C37}$ for every $\overline{C37}$ bin of 0.02. Results are based on **control** and **no MWI** and cover the time period 11 June to 31 July 2017.

for negative FG dep values with 3.1 K for $|\text{FG dep}| = 3$ K. These differences between observation error (symmetric cloud amount) and too moist or too dry areas (negative or positive FG dep) motivate a closer look at the observation error model and hence $\overline{C37}$, especially in scenes characterized by a low cloud amount.

The observation error model is a simplification of the behaviour of standard deviation of first guess departure as a function of $\overline{C37}$ [Geer and Bauer, 2011] . For clear and cloudy situations a different observation error is assigned depending on $\overline{C37}$. For example, for 37v GHz channel of SSMIS-F17 in IFS cycle 45R1 an observation error of σ_{clear}= 1.8 K is assigned to clear scenes with $\overline{C37} < 0.02$ and σ_{cloudy}= 18 K to cloudy scenes with $\overline{C37} > 0.42$, as illustrated in Fig. 10. For $0.02 \leq \overline{C37} \leq 0.42$ the observation error increases linearly with $\overline{C37}$ from 1.8 K to 18 K.

If the calculation of $\overline{C37}$ (and hence observation error) is affected by biases, these could potentially affect how much drying or moistening occurs, and hence promote a drying in the analysis. Two potential candidates which are believed to introduce biases in the observation error model are discussed in more detail in the next sections: bias correction of $\overline{C37}$ (section 4) and water vapour effects on $\overline{C37}$ (section 5).

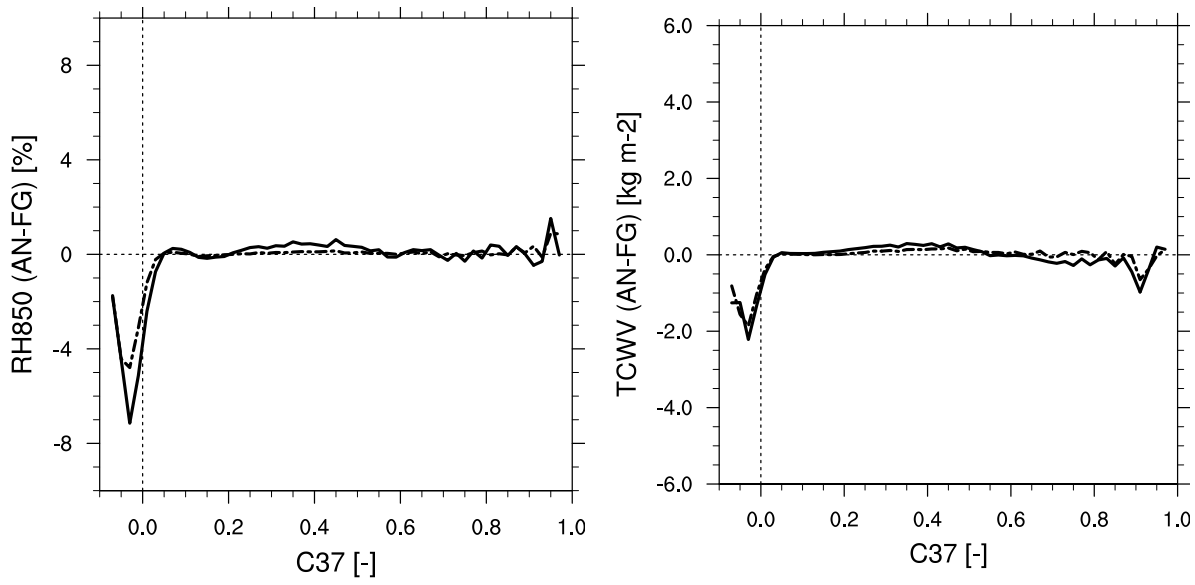

(a) Relative humidity at 850hPa

(b) Total Column Water Vapour

Figure 8: Binned mean (solid line) and median (dashed-dotted line) a) increment in relative humidity at 850 hPa and b) increment in TCWV (total column water vapour) as a function of $\overline{C37}$. Results are from **control** and cover a time period 11 June to 31 July 2017.

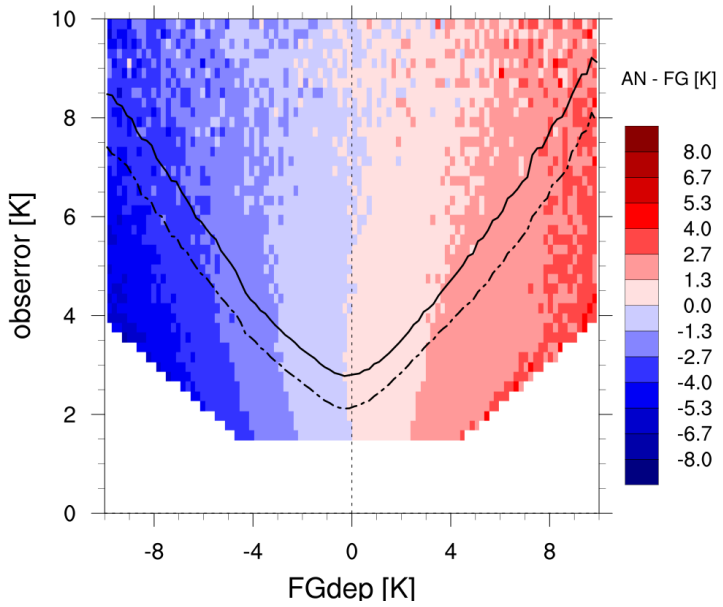

Figure 9: (i) Line plot: Binned mean (solid line) and median (dashed line) in observation error as a function of first guess departure (FG dep) at 37 v GHz from SSMIS-F17. (ii) Colour contours: analysis increment [K], binned for every 0.2 K FG departure x 0,2 K observation error. Blue colours correspond to the first guess being larger than analysis and red colours vice versa. Results are from **control** and cover a time period 11 June to 31 July 2017.

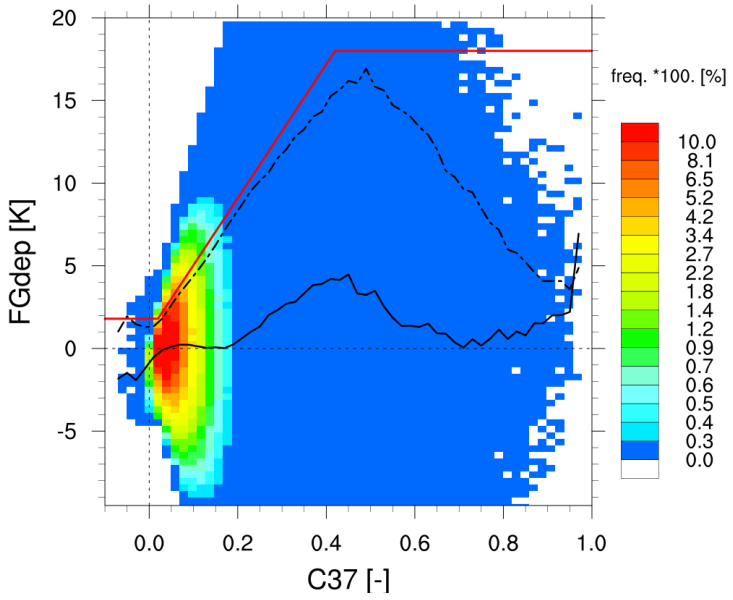

Figure 10: (i) Line plot: Binned mean (solid line) and standard deviation (dashed-dotted line) of the first guess departure (FG dep) at 37 v GHz from SSMIS-F17 as a function of $\overline{C37}$. (ii) Colour contours: frequency of occurrence [%], binned for every 0.02 $\overline{C37}$ x 0.4 K FG departure. Note that the y-axis is asymmetrical to focus on the behaviour of standard deviation with $\overline{C37}$. The missing -10 to -20 K range is essentially a mirror image of the +10 to +20 K range. Red line illustrates the observation error model. Results are from **control** and cover a time period 11 June to 31 July 2017.

4 Bias correction of cloud amount $\overline{C37}$

As shown in Eq. 2 the calculation of the first guess and observed cloud amount depends on the polarisation difference in brightness temperatures measured at 37 GHz and its cloud- and precipitation free counterpart. However, until now non-biascorrected brightness temperatures have been used to compute $C37_{obs}$ even though mean biases are about 1.8 K for 37 GHz, v-polarised and 3.9 K for 37 GHz, h-polarised. An experiment (**exp. 1**) has been setup to test if the drying effect changes when bias corrected $C37_{obs}$ values (and hence bias corrected $\overline{C37}$ values) are used. It can be seen in Fig. 11 that the mean in FG departures is still below zero for negative values in $\overline{C37}$ as it was before (Fig. 10). Hence, using biascorrected brightness temperatures for the computation of $C37_{obs}$ is unlikely to make a difference for the additional drying effect.

5 Water vapour effects on cloud amount $\overline{C37}$

The bias correction of $C37_{obs}$ only affects the numerator in Eq. (2), whereas the denominator, the polarisation difference in the cloud- and precipitation free atmosphere, has not been modified. As noted earlier, the same denominator is used for the calculation of C37 for observations and for the first guess (FG). This is because brightness temperatures in a cloud- and precipitation free atmosphere cannot be measured when it is cloudy. However, an approximate reconstruction of such observed clear sky brightness temperatures is possible if the surface emissivity is well known and the moisture field can be estimated from observations.

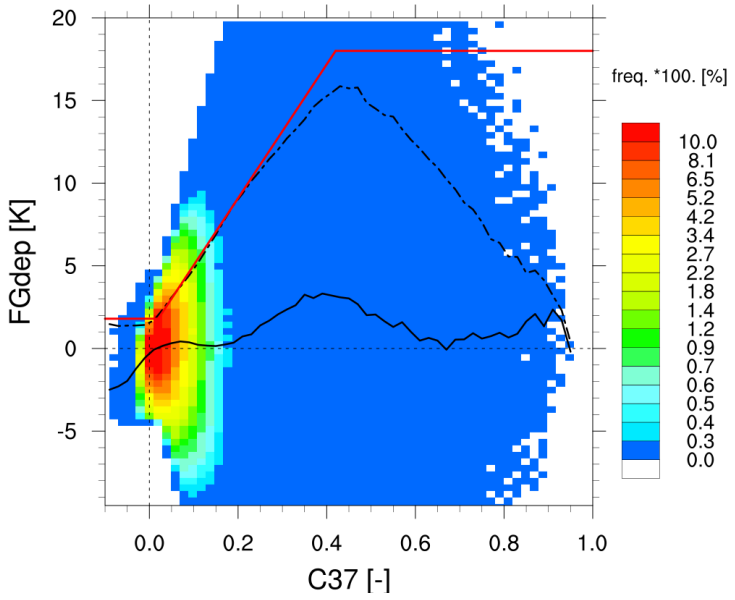

Figure 11: (i) Line plot: Binned mean (solid line) and standard deviation (dashed-dotted line) of the first guess departure (FG dep) at 37 v GHz from SSMIS-F17 as a function of $\overline{C37}$. (ii) Colour contours: frequency of occurrence [%], binned for every 0.02 $\overline{C37}$ x 0.4 K FG dep. Note that the y-axis is asymmetrical to focus on the behaviour of standard deviation with $\overline{C37}$. The missing -10 to -20 K range is essentially a mirror image of the +10 to +20 K range. Red line illustrates the observation error model. Results are for the active all-sky experiment using bias corrected $\overline{C37}$ (**exp. 1**) and cover a time period 11 June to 31 July 2017.

To reconstruct clear sky brightness temperatures it is possible to exploit a simple retrieval of total column water vapour using brightness temperatures at 22 GHz, vertically polarised. This reconstruction has the potential to deliver more accurate observed clear sky brightness temperatures compared to just using the first guess. If we assume that the observed and modelled moisture field differ in some situations one can easily see that using modelled clear sky brightness temperatures for an observed atmosphere causes a bias in the computation of $C37_{obs}$. For example, a modelled atmosphere which has a higher humidity than what is observed translates into a smaller clear-sky polarisation difference $T_v^{clr} - T_h^{clr}$ which results in a decreased value in $C37_{obs}$ [see Eq. (2)]. In other words, if $C37_{obs}$ is calculated using FG clear sky conditions which are too moist, then the observation error is decreased and the influence on the analysis field of those observations is increased. This bias only matters when the all-sky polarisation difference is in the same order as the clear-sky polarisation difference, which is the case when it is not very cloudy. That means humidity differences between first guess and observations only play an important role for samples with a small symmetric cloud amount, which are quite numerous according to Fig. 11.

To account for differences in the modelled and observed moisture field, a reconstruction of the clear sky polarisation difference for first guess (FG) and observations has been tested on top of using bias-corrected brightness temperatures for the calculation of the all-sky polarisation difference at 37 GHz (section 4). For this purpose the approximate radiative transfer equation:

$$T_{v,h} = T_a \left(1 - \tau^2 (1 - \varepsilon_{v,h})\right), \tag{3}$$

with the brightness temperature at vertical/ horizontal polarisation, $T_{v,h}$, the atmospheric transmittance, τ, the surface emissivity at vertical/ horizontal polarisation, $\varepsilon_{v,h}$, and T_a = 280 K is used to calculate the

polarisation difference at 37 GHz:

$$T_{37,v} - T_{37,h} = T_a \cdot \tau_{37}^2 (\varepsilon_v - \varepsilon_h). \tag{4}$$

Here, the temperature T_a represents the atmospheric temperature at an effective height of the absorbing layer [Grody et al., 1990], which has been chosen to be 280 K. The transmittance can be expressed in terms of a mass extinction coefficient, k [$m^2\,kg^{-1}$], and the density along the path of the satellite [Petty, 2006, section 7.2.2]. In an atmosphere without clouds and ignoring some very minor trace gases, moisture is the sole control over the transmittance window at microwave frequencies along the path of the satellite which results in:

$$\tau_{clr} = \exp\left(\frac{-k^{va} \cdot \mathrm{TCWV}}{\cos\theta}\right), \tag{5}$$

with the viewing satellite angle, θ, the mass extinction coefficient of water vapour, k^{va}, and the total column water vapour, TCWV [$kg\,m^{-2}$]. Eq. (5) inserted into eq. (4) and considering an atmosphere without clouds gives:

$$T_{37,v}^{clr} - T_{37,h}^{clr} = T_a \cdot \exp\left(\frac{-2k_{37}^{va} \cdot \mathrm{TCWV}}{\cos\theta}\right)(\varepsilon_v - \varepsilon_h) := P37^{clr}, \tag{6}$$

with $P37^{clr}$ being the clear sky polarisation difference.

A reconstruction of the clear-sky polarisation difference should contain the same amount of information and uncertainties for observations and FG, making them more equivalent than when using the model atmosphere to compute $T_{37,v}^{clr} - T_{37,h}^{clr}$ for observations and FG. In order to calculate a reconstructed clear-sky polarisation difference with eq. (6) the emissivity, ε, the mass extinction coefficient at 37 GHz, k_{37}^{va}, the zenith angle, θ, and the TCWV have to be known.

The surface emissivity over ocean is calculated using an emissivity model for the first guess. Assuming that those values are quite accurate allows to use the same surface emissivity values for first guess and observations. The TCWV, however, can differ between first guess and observations. In other words, the first guess TCWV should not be used for observations, especially when differences in moisture are large and cloudiness low. As mentioned before, the difference in moisture between FG and observation motivated us to find a better estimate of the observed clear-sky polarisation difference in the first place.

The first step is to approximate the TCWV with a simple retrieval using the brightness temperature at 22 GHz, v-polarised $T_{22,v}$, according to Karstens et al. [1994]:

$$\mathrm{TCWV} = A \cdot \ln(T_a - T_{22,v}) + B, \tag{7}$$

with coefficients, A and B. A linear regression between the FG TCWV vapour and the modelled brightness temperature at 22 GHz, vertically polarised from SSMIS-F17 over a time period between 11 June, 00 UTC and 31 July 2017, 12 UTC using the output from the active all-sky experiment with bias-corrected $\overline{\mathrm{C37}}$ (**exp.1**) yields the coefficients A =-32.339 and B = 153.436.

The second step is to calculate the ratio between the mass extinction coefficient of water vapour, k^{va}, and the zenith angle, θ, by using eq. (6) for the FG clear-sky polarisation difference, $(T_{37,v}^{clr} - T_{37,h}^{clr})_{FG} = P37_{FG}^{clr}$, and transposing it to:

$$\frac{-2k_{37}^{va}}{\cos\theta} = \frac{\ln\left(\dfrac{P37_{FG}^{clr}}{T_a \cdot (\varepsilon_v - \varepsilon_h)}\right)}{\mathrm{TCWV}_{FG}}. \tag{8}$$

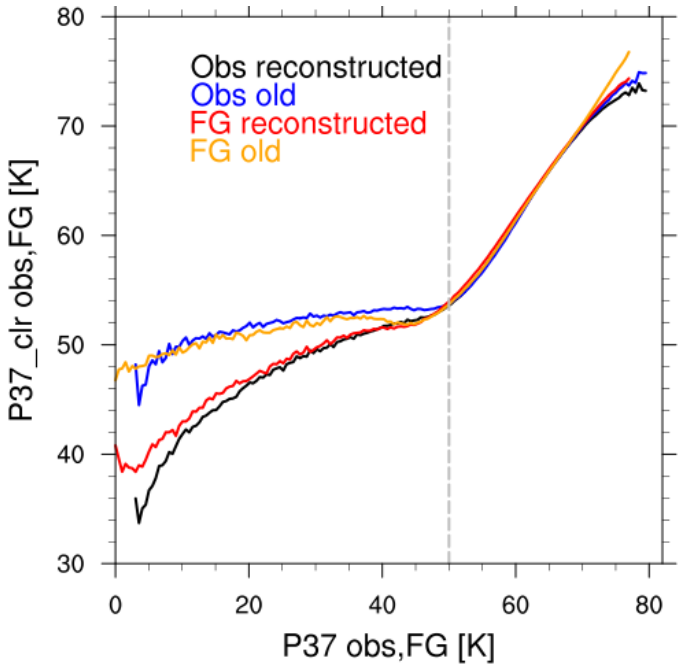

Figure 12: Median in clear-sky polarisation difference at 37 GHz, $P37^{clr}$, versus all-sky polarisation difference at 37 GHz, P37, for the active all-sky experiment using bias-corrected values of $\overline{C37}$ (**exp. 1**). The median is taken for every 0.5 P37 bin and over the time period 11 June to 31 July 2017. The colours refer to the different combinations of P37 using the reconstructed clear-sky polarisation difference $P37^{clr}_{rec}$ for observations (black) and for FG (red) and the non-reconstructed clear-sky polarisation difference (based on the first guess) for observations (blue) and for FG (yellow). The grey dashed line represents a reference line.

Finally, the reconstructed clear-sky polarisation difference, $P37^{clr}_{rec}$, can be computed for FG and observations by inserting eq. (8) into eq. (6):

$$P37^{clr}_{rec} = (T^{clr}_{37,v} - T^{clr}_{37,h})_{rec} = T_a \cdot \left(\frac{P37^{clr}_{FG}}{T_a \cdot (\varepsilon_v - \varepsilon_h)} \right)^{\frac{A \cdot \ln(T_a - T_{22,v}) + B}{\mathrm{TCWV}_{FG}}} \cdot (\varepsilon_v - \varepsilon_h). \tag{9}$$

Here, TCWV_{FG} is the first guess total column water vapour. For the reconstructed clear-sky polarisation difference for FG , $P37^{clr}_{rec_{FG}}$, $T_{22,v}$ is used from the FG field, whereas for the reconstructed clear-sky polarisation difference for observations , $P37^{clr}_{rec_{obs}}$, the observed $T_{22,v}$ is used in eq. (9).

As already mentioned, reconstructed clear-sky brightness temperatures/ polarisation differences cannot be used under all conditions. The reconstruction only makes sense with little cloud, as justified by Fig. 12. This illustrates that the reconstruction of the clear-sky polarisation is affected by clouds as shown by large differences between reconstructed and non-reconstructed values of clear-sky polarisation difference in cloudy conditions. The all-sky polarisation difference at 37 GHz, P37, is a relatively good measure of cloudiness whereas its cloud- and precipitation free counterpart, $P37^{clr}$, is a good measure for moisture (when it is not biased). The smaller P37 or $P37^{clr}$ the more clouds or moisture are in the atmosphere, respectively. The non-reconstructed clear-sky polarisation difference for FG as a function of the all-sky polarisation difference (yellow line) is by definition not biased, but all the other combinations of all-sky polarisation difference and clear-sky polarisation difference are biased in some way (for more information on the different combinations/lines in Fig. 12 see Tab. 3). The reconstructed clear-sky polarisation

difference for FG (red line) differs quite significantly from the non-reconstructed clear-sky polarisation difference for FG (yellow line) for very cloudy situations (small P37). A similar behaviour holds true for reconstructed [black line] and non-reconstructed [blue line] clear-sky polarisation difference for observations. This indicates that the reconstructed values of clear-sky polarisation difference should only be used under conditions with a small cloud content. Therefore, a threshold of P37 at 50 K [dashed grey line] has been chosen to decide between applying the reconstructed clear-sky polarisation difference (i.e. all samples with P37 greater than the threshold) or the non-reconstructed (original) clear-sky polarisation difference.

Table 3: Description of the different coloured lines in Fig. 12.

colour	**description**
black line	reconstructed clear-sky polarisation difference for observations ($P37^{clr}_{rec_{obs}}$) as a function of the observed all-sky polarisation at 37 GHz
blue line	non-reconstructed clear-sky polarisation difference for observations ($P37^{clr}_{obs}$) as a function of the observed all-sky polarisation at 37 GHz
red line	reconstructed clear-sky polarisation difference for first guess ($P37^{clr}_{rec_{FG}}$) as a function of the first guess all-sky polarisation difference at 37 GHz
yellow line	non-reconstructed clear-sky polarisation difference for first guess ($P37^{clr}_{FG}$) as a function of the first guess all-sky polarisation difference at 37 GHz

For values larger than P37 equals 50 K the reconstructed FG clear-sky polarisation difference matches very well the original one even though some possible biases could be introduced in the calculation of the reconstructed clear-sky polarisation difference. A particular issue would be using the brightness temperature at 22 GHz, v-polarised, $T_{22,v}$ to retrieve TCWV. As been shown before, the TCWV retrieval becomes biased when it is very cloudy and, hence, the calculation of reconstructed clear-sky polarisation difference becomes biased, too. Another bias could be introduced through the assumption that the model emissivity represents observed values, which is a reasonable assumption even though emissivity values for breaking waves under very windy conditions are difficult to model. Nevertheless, even though these biases could be introduced in the calculation of the clear-sky polarisation difference they are applied in a more symmetric way for both reconstructed clear-sky polarisation difference values of FG and observations and are much more comparable to each other than using an error-free value for the clear-sky polarisation difference for FG but a defective value for the clear-sky polarisation difference for observations. Without the calculation of reconstructed clear-sky polarisation differences, $C37_{obs}$ is more biased than $C37_{FG}$.

Fig. 13 shows the symmetric cloud amount as a function of FG departures. Using a more symmetric approach for the reconstructed clear-sky polarisation difference helps improve the calculation of the symmetric cloud amount, $\overline{C37}$. The symmetric cloud amount which applies reconstructed clear-sky polarisation difference values (red line in Fig. 13) is more symmetric for same absolute values of FG departures than the original symmetric cloud amount (black line in Fig. 13). Here, applying reconstructed clear-sky polarisation differences gives a small increase in low symmetric cloud amount values. Especially for FG departures between -4 K and 0 K, an increase in the reconstructed symmetric cloud amount can be seen. Furthermore, it is shown that the reconstructed symmetric cloud amount is less often below $\overline{C37} = 0.02$ whereas the original symmetric cloud amount is below that value for FG departures between -2 K and 1 K. The value of $\overline{C37} = 0.02$ is of special interest as it is the upper threshold for the clear-sky observation error of 1.8 K. Above that value the observation error linearly increases up to 18 K at $\overline{C37} =$

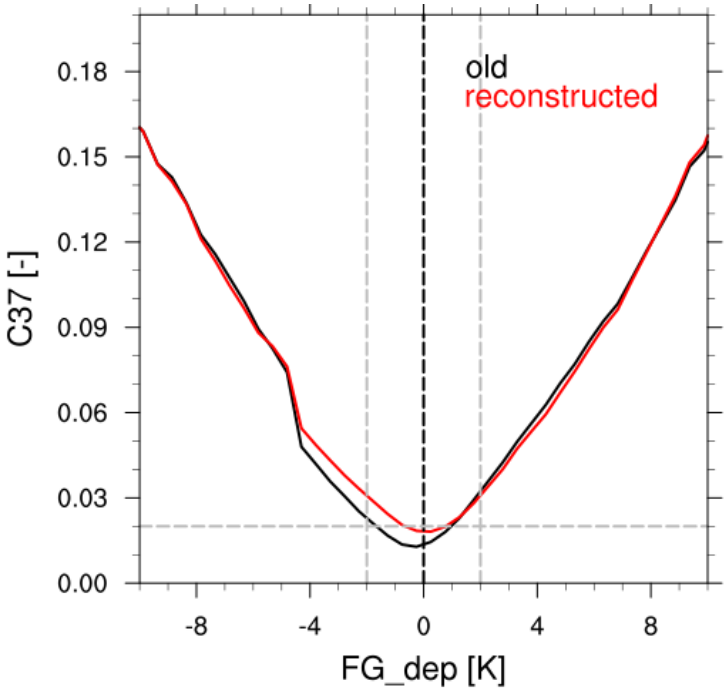

Figure 13: Median symmetric cloud amount, $\overline{C37}$, versus FG departure [K] in 37 GHz for active all-sky experiment using bias-corrected values of $\overline{C37}$ (**exp. 1**). The median is taken for every 0.5 FGdep bin and over the time period 11 June to 31 July 2017. The black line refers to original values in $\overline{C37}$ and the red line to the reconstructed calculation of $\overline{C37}$ using reconstructed clear-sky polarisation difference ($P37^{clr}_{rec}$) values for conditions which are not very cloudy. The grey dashed lines represent reference lines.

0.42 (see section 3). In other words, a small increase in low symmetric cloud amount values leads to a moderate increase in the observation error, which could reduce the weight of samples that lead to drying in the analysis.

That the reconstruction of the clear-sky polarisation difference treats $C37_{obs}$ and $C37_{FG}$ in a more symmetric way can also be seen in Fig. 14, where the standard deviation and mean in FG departures are displayed as a function of symmetric cloud amount, $\overline{C37}$, for the active all-sky experiment using bias-corrected values of $\overline{C37}$ and reconstructed values of clear-sky polarisation difference, $P37^{clr}_{rec}$ (**exp. 2**). Here, the mean FG departure is close to 0 and the spread around the mean is similar for negative and positive FG departures for $\overline{C37} < 0.2$ (seen by frequency of occurrence), which is a good indicator that the reconstructed $\overline{C37}$ inhibits the previous asymmetry of $C37_{obs}$ and $C37_{FG}$. This is especially true for negative values of $\overline{C37}$, where before (Fig. 11) the mean FG departure decreased to negative values.

6 Results

6.1 Impact of modified observation error model

As shown in section 1 the additional drying effect disappeared in humidity observations from radiosondes (over land) through the assimilation of the 150/166 GHz channels. However, the drying effect associated with conditions of low cloud amount over ocean is still present. Hence, we must check if the implementation of the bias correction of C37 and the additional usage of reconstructed $P37^{clr}_{rec}$ values in the

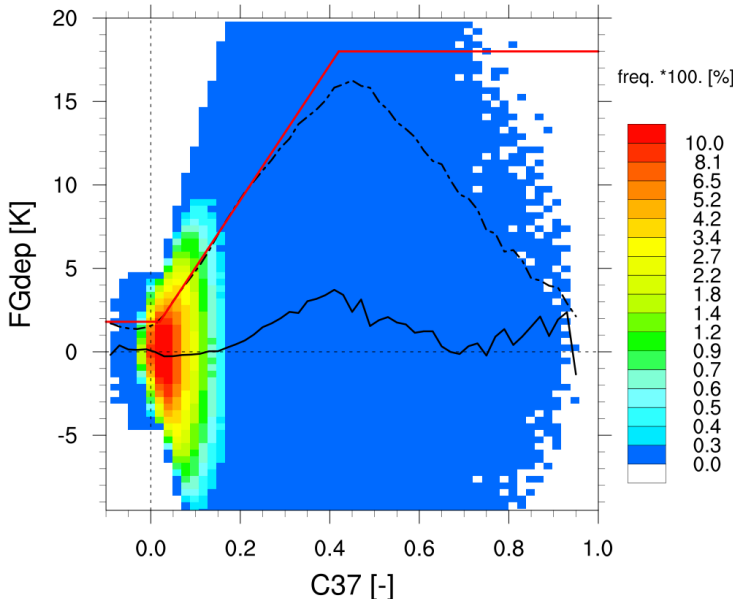

Figure 14: (i) Line plot: Binned mean (solid line) and standard deviation (dashed-dotted line) of the first guess departure (FG dep) at 37 v GHz from SSMIS-F17 as a function of $\overline{C37}$. (ii) Colour contours: frequency of occurrence [%], binned for every 0.02 $\overline{C37}$ x 0.4 K FG dep. Note that the y-axis is asymmetrical to focus on the behaviour of standard deviation with $\overline{C37}$. The missing -10 to -20 K range is essentially a mirror image of the +10 to +20 K range. Red line illustrates the observation error model. Results are for the active all-sky experiment using bias corrected $\overline{C37}$ and reconstructed values of $P37^{clr}_{rec}$ (**exp. 2**) and cover a time period 11 June to 31 July 2017.

observation error model really improves the humidity field over ocean.

For this purpose we compare the analysis relative humidity at 850 hPa of the **active all-sky** experiments with the **passive all-sky** experiment over a time period from 11 June 2017, 00 UTC to 31 July 2017, 12 UTC at observation locations. As illustrated in Table 4 using a bias-corrected $\overline{C37}$ seems to increase the mean drying effect from -0.29% (**control**) to -0.49% (**exp. 1**). Applying additionally the reconstructed $P37^{clr}$ to the calculation of $\overline{C37}$ (**exp. 2**) decreases the mean drying effect to -0.27%. As it can be seen in Fig. 15 the local differences between **control** and **exp. 2** are quite subtle, which is reflected in the values of the mean change. However, looking only at global mean changes might not be the best indicator of how well the changes in the observation error model address the additional drying effect for scenes with low cloud amount.

Fig. 16 shows nicely that the difference in the analysis relative humidity at 850 hPa between **exp. 2** and the passive all-sky experiment (**no MWI**) is not as reduced for small values in $\overline{C37}$ as compared to the difference between **control** and **no MWI** (Fig. 7). This improvement in the drying effect was exactly what was anticipated by taking care of water vapour effects of $\overline{C37}$ inside the observation error model for nearly cloud-free conditions.

6.2 Observational verification

To verify the experiments for the short-range forecast, fits to other independent observations are checked. Observational fits which are sensitive to humidity and temperature, like the Advanced Microwave Sound-

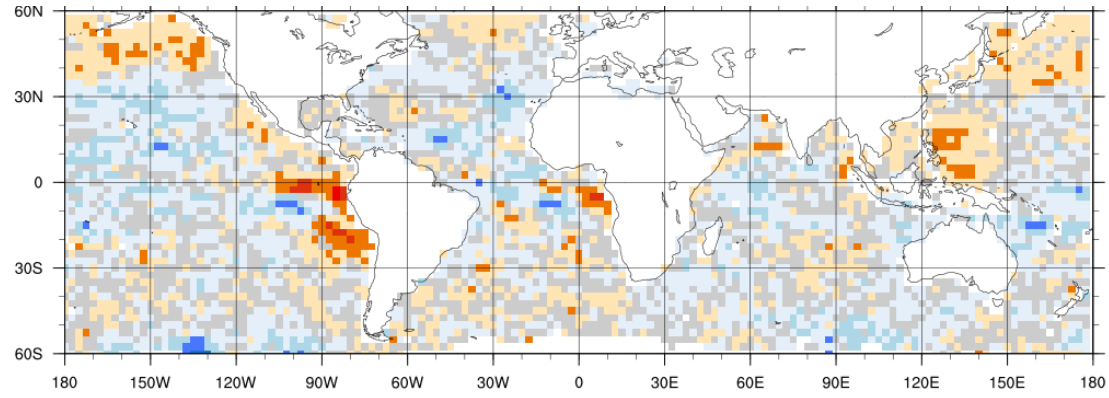

(a) **control**

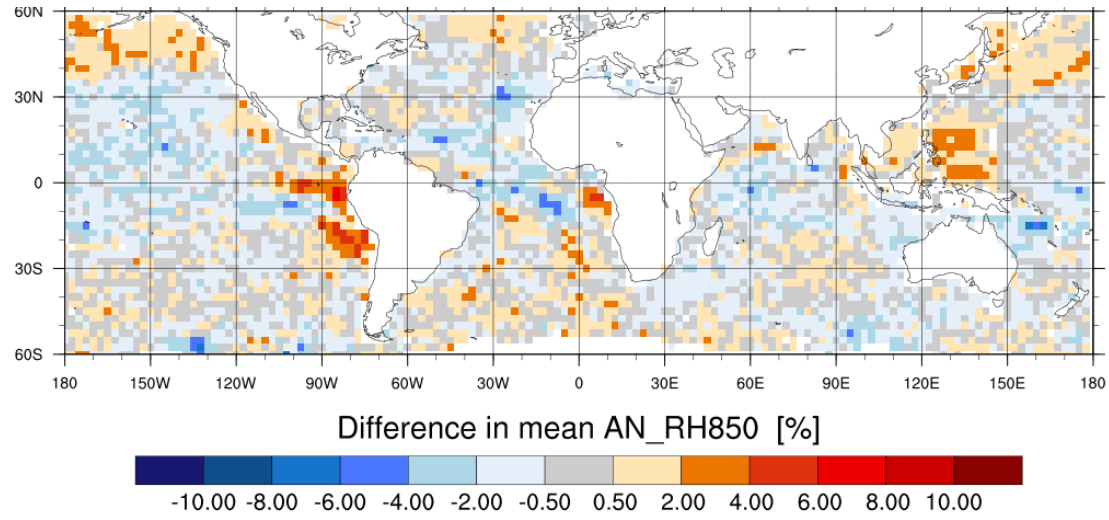

(b) **exp. 2**

Figure 15: Difference in time-mean analysis humidity at 850 hPa between active all-sky experiments and passive all-sky experiment (**no MWI**). As Fig. 2 but for 45R1 experiments, which assimilate the imager channels of SSMIS-F17 actively or passively, only. The means are taken over the time period 11 June to 31 July 2017.

ing Unit-A (AMSU-A, from Aqua, NOAA-15, NOAA-16, NOAA-18, NOAA-19, Metop-A and Metop-B; Fig.17b) or the Advanced Technology Microwave Sounder (ATMS, from NPP) show mostly a neutral effect from both modifications (**exp. 1** and **exp. 2**). Wind observations from Atmospheric Motion Vectors (AMVs; Fig.17d) and wind profiles, and clear sky radiances (Fig.17a) show a neutral effect, too. Some water vapour sensitive channels of CRIS (Fig.17c) show a small improvement for **exp. 2**. In summary, fits to independent observations are mostly neutral with **exp. 2** showing slightly better fits.

Interestingly, the number of observations for SSMIS-F17 changes in **exp. 1** and **exp. 2** compared to the **control**, with the **control** having the highest number of observations. This is due to VarQC rejecting more data for both experiments. Modifications to C37 change the observation errors assigned and, hence, have an impact on how many observations pass the FG departure check. Fits to SSMIS-F17 using the same sample of data for **exp. 2** and **control** (Fig. 18) reveals that **exp. 2** improves the fit by up to 2.3% for 92 Ghz, v-pol (channel 17) in the Tropics, where high amounts of water vapour prevail and, hence, using

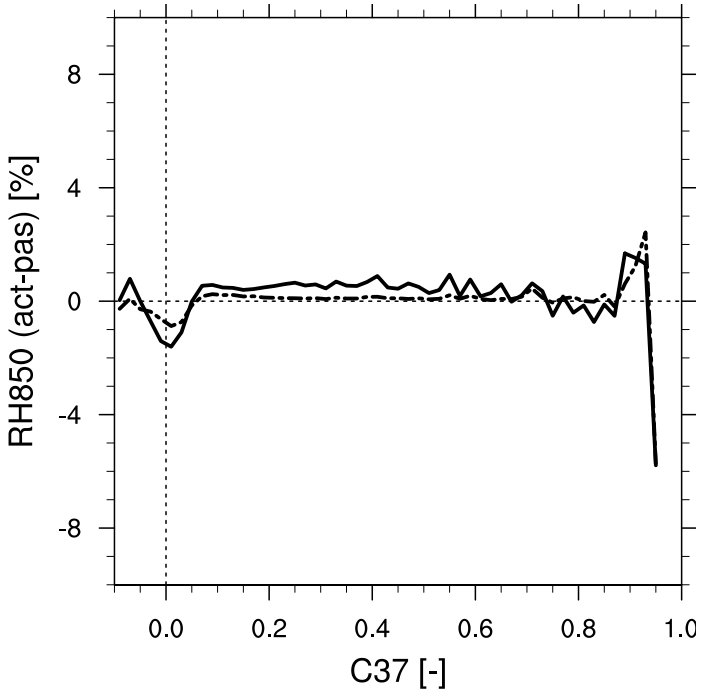

Figure 16: Binned mean (solid line) and median (dashed-dotted line) difference in analysis relative humidity at 850 hPa between the active and passive 45R1 all-sky experiment as a function of $\overline{C37}$ for every $\overline{C37}$ bin of 0.02. Results are based on the **exp. 2** configuration and cover the time period 11 June to 31 July 2017.

a better description of water vapour inside the observed clear-sky polarisation difference at 37 GHz shows the best results.

6.3 Forecast scores

To study how global forecast scores are affected we look at the change in the root-mean-square of forecast error (RMSE) of different variables. A decrease in RMSE would usually be interpreted as an improvement and an increase in RMSE as a degradation in forecast scores. However, as shown later one has to

Table 4: Mean analysis relative humidity [%] at 850 hPa for active all-sky experiments compared to passive all-sky experiment (**no MWI**). Mean and standard error are computed over the time period 11 June to 31 July 2017 at observation locations.

configuration	mean $\pm$ std. err.	difference to **no MWI**
control	69.84 $\pm$ 0.18	-0.29 $\pm$ 0.02
exp. 1: bias-corrected $\overline{C37}$	69.63 $\pm$ 0.19	-0.49 $\pm$ 0.02
exp. 2: bias-corrected $\overline{C37}$ + reconstructed P37 $^{clr}_{rec}$	69.85 $\pm$ 0.18	-0.27 $\pm$ 0.02
no MWI: as **control**	70.13 $\pm$ 0.18	

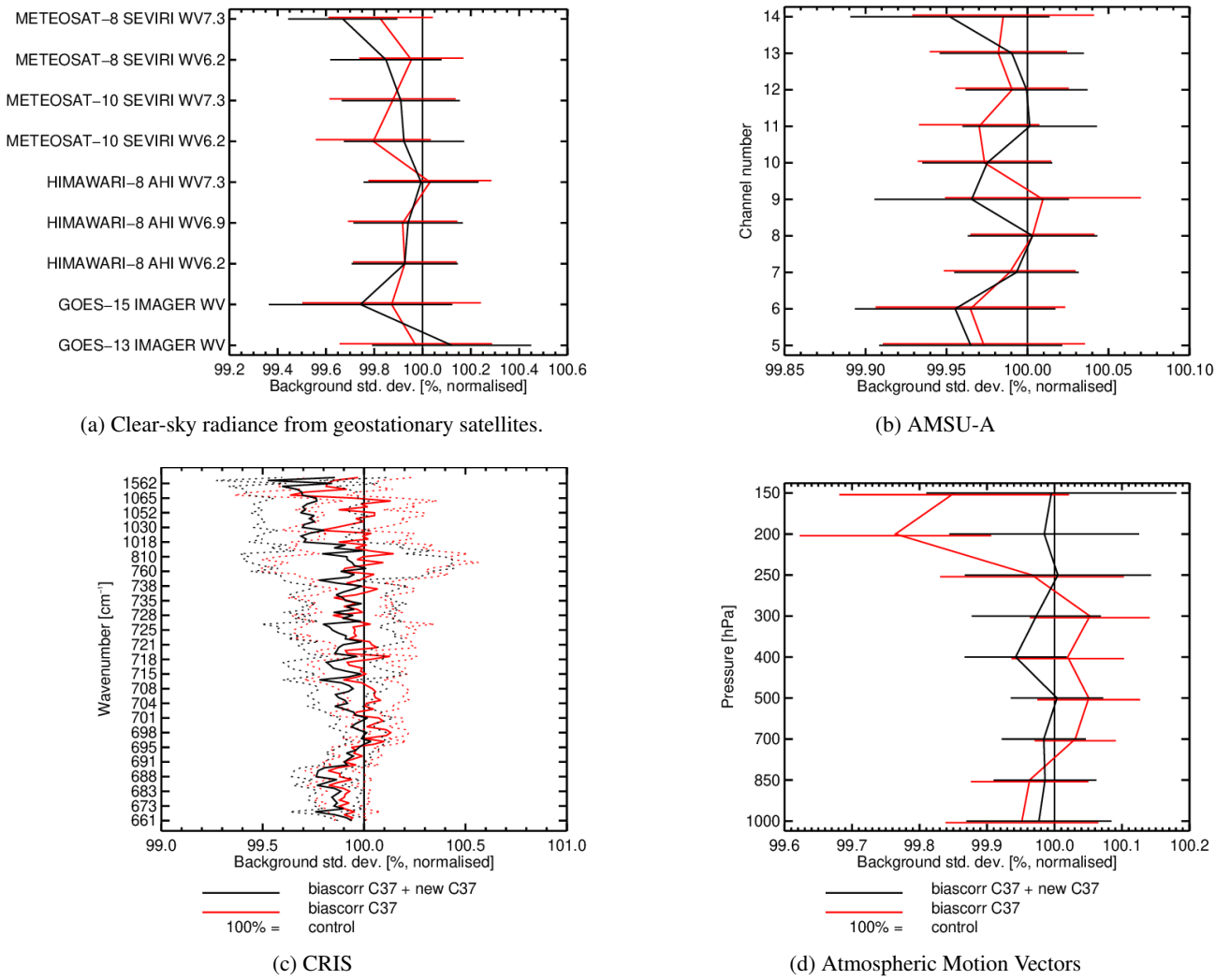

(a) Clear-sky radiance from geostationary satellites.

(b) AMSU-A

(c) CRIS

(d) Atmospheric Motion Vectors

Figure 17: Normalised difference in standard deviation of first-guess departures between **exp. 1** (red), **exp. 2** and **control** for different instruments. The normalisation is done with results from control. Values less than 100% would indicate beneficial impacts from the experiments. The horizontal bars indicate 95% confidence range. Results cover the time period from 11 June to 31 July 2017.

be careful with this interpretation. Fig. 19 shows the zonal averages in normalised difference in RMSE in humidity between **exp. 2** and **control**. Up to T+24 h the RMSE in humidity seems to be increased (degraded) in the lower troposphere, mainly in the winter hemisphere (southern hemisphere) with the largest apparent degradation happening at T+12 h. In fact, the T+12 h own analysis RMSE actually represents the RMS of the analysis increment. That means if the analysis increments become larger, the RMSE will also appear large. No changes in RMSE are seen for temperature and wind.

A reason for this increase in RMSE in the winter hemisphere could be due to a change in the analysis instead of the forecast, which would prevent a spread in time. To test this hypothesis we have looked at forecast scores verified with the operational analysis instead of own analysis. A slight reduction in RMSE can be seen for humidity (Fig.20) and temperature (not shown). That means, for **exp. 2** mostly the variability of the analysis is increased with minor mean changes in humidity and temperature for the

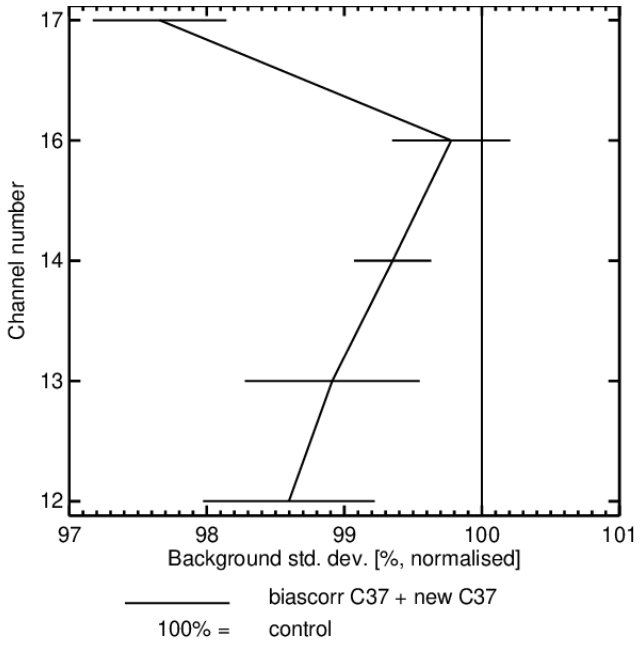

Figure 18: Normalised difference in standard deviation of first-guess departures between **exp. 2** (black) and **control** for the same sample of SSMIS-F17 data in the Tropics (20°S - 20°N). The normalisation is done with results from control. Values less than 100% would indicate beneficial impacts from the experiments. The horizontal bars indicate 95% confidence range. Results cover the time period from 11 June to 31 July 2017.

short-range forecast up to T+24 h.

7 Summary

The IFS tends to generate a lower atmosphere that is a bit too dry compared to observations. The model climate has a too dry analysis even without the assimilation of satellite observations, as compared to radiosonde humidity observations. The assimilation of microwave imagers has been shown to increase this drying slightly. Results from an experiment withholding most satellite observations suggest that the "model climate" is about 4×10^{-5} kg kg^{-1} too dry at 850 hPa, which is in the range of the dry biases seen by experiments without assimilating SSMIS-F17.

The additional drying effect seen through the assimilation of microwave imagers has been decreased significantly in the past by two modifications of the IFS: mainly through the addition of 150/166 GHz in IFS cycle 46R1 and partly through the introduction of an upgraded humidity background error model in IFS cycle 43R3. In this report we study two hypotheses for the remaining drying of the analysis coming from the assimilation of microwave imagers linked to conditions with small cloud amount .

Both hypotheses for the additional drying are based on the way the observation errors are assigned using the symmetric cloud amount, $\overline{C37}$. Examining the first hypothesis, using bias corrected $\overline{C37}$ values (**exp. 1**) has shown no profound difference to the additional drying effect. The second hypothesis is linked to the finding that the drying mainly occurs in almost cloud-free scenes. It was found that the representation of water vapour in the observation error model in these cases could be related to the dry bias. Using reconstructed values for clear sky brightness temperatures at 37 GHz (**exp. 2**) as part of the

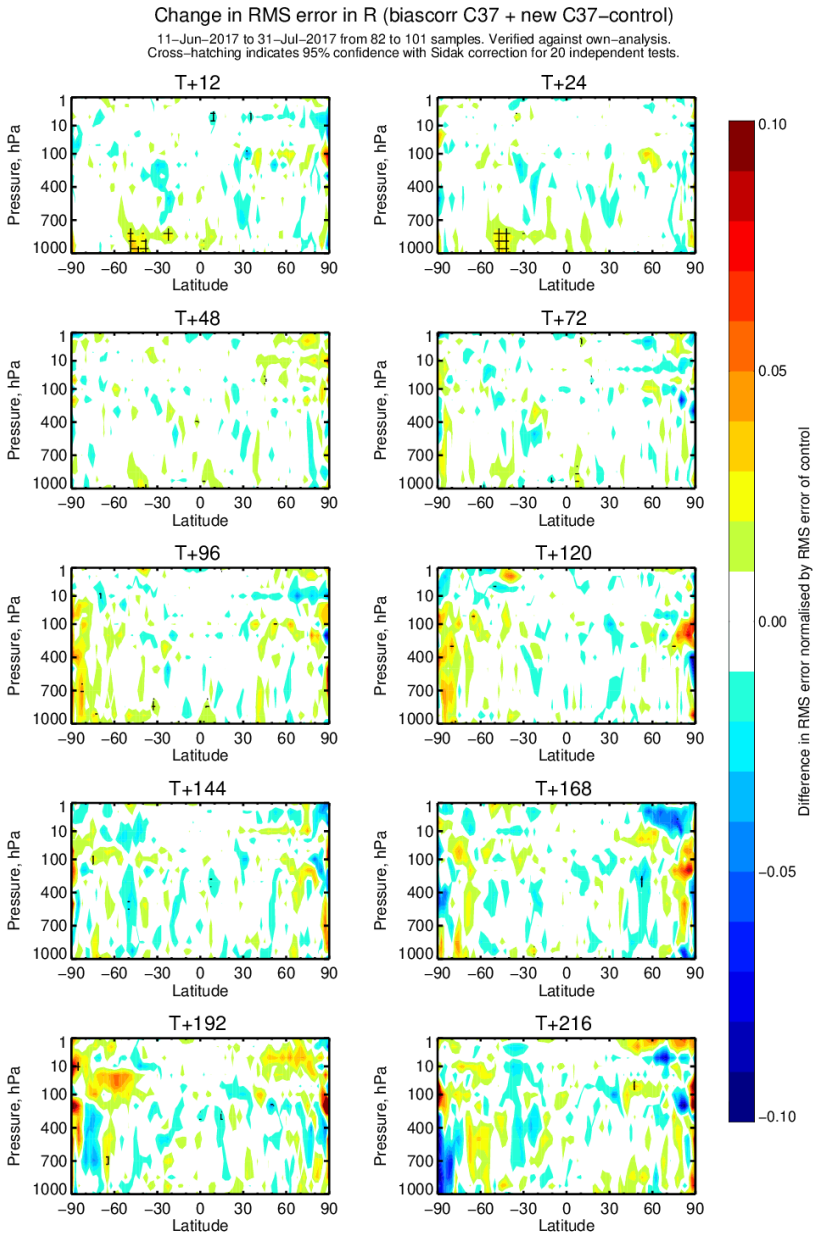

Figure 19: Zonal averages of differences in RMSE in humidity between **exp. 2** and control normalised by **control** and verified against own analysis at different height levels for different forecast times. Blue colours represent a decrease in RMSE and red colours and increase in RMSE for **exp. 2**. Results cover the time period from 11 June to 31 July 2017.

observation error model allowed a more symmetric treatment of how water vapour affects the clear sky polarisation difference at 37 GHz ($P37^{clr}$) for observations and first guess.

At first, the modifications to the observation error model seem to have hardly any effect on improving the additional drying effect when comparing the analysis relative humidity at 850 hPa from experiments assimilating microwave imager SSMIS-F17 with an experiment, which does not. Looking at conditions with low cloud amount showed, however, almost no drying effect in analysis relative humidity at 850 hPa

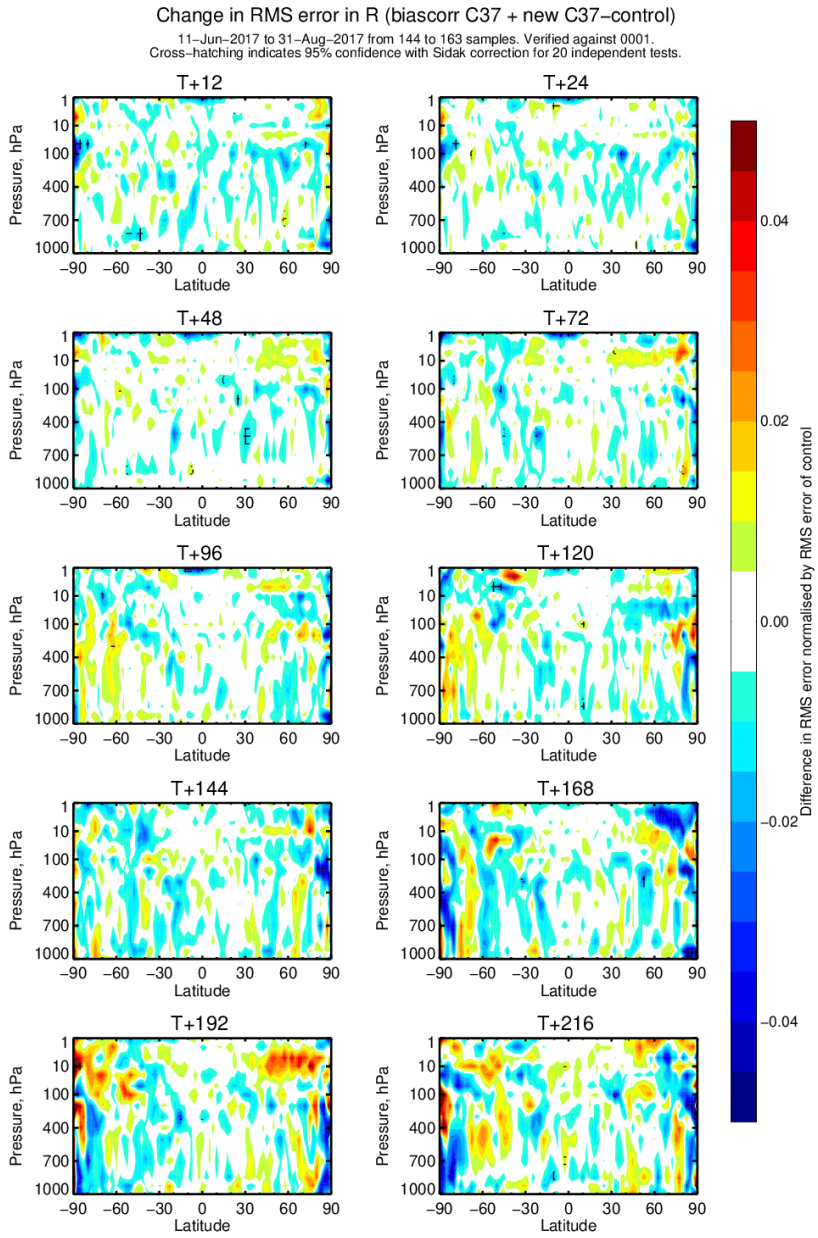

Figure 20: Zonal averages of differences in RMSE in humidity between **exp. 2** and control normalised by **control** and verified against operational analysis at different height levels for different forecast times. Blue colours represent a decrease in RMSE and red colours and increase in RMSE for **exp. 2**. Results cover the time period from 11 June to 31 July 2017.

for **exp. 2**. This outcome is in line with what has been anticipated by modifications done to **exp. 2**.

Experimentation with the modified observation error model (bias correction of $\overline{\text{C37}}$ + reconstructed P37^{clr}, **exp. 2**) shows mostly a neutral impact on short-range forecasts, as evaluated through background departure statistics for other assimilated observations. However, improved fits could be seen for SSMIS-F17, especially in the tropics, when the same sample of observations is used. Introducing the modified observation error model decreased the number of SSMIS-F17 being assimilated as these changes led to

more observations being rejected through the quality control. Forecast scores have shown an increase in own analysis RMSE in humidity for **exp. 2**. However, this has been identified to be a change in the analysis and short-range forecast. Medium-range global forecast scores are mostly unaffected by using a bias correction of $\overline{\text{C37}}$ and reconstructed P37^{clr}.

When using the reconstructed clear-sky radiances one has to be careful in setting the needed parameters in the simple water vapour retrieval, as those are very sensitive depending on which sensor it applies to. Hence, in our study we have only tested using reconstructed clear-sky radiances for one microwave imager (SSMIS-F17) for a certain time period in the active all-sky experiment. For an operational implementation one would have to make the retrieval of the coefficients in Eq. (7) more dynamic depending on the time and microwave imager instrument to avoid high manual maintenance when sensor characteristics change.

In summary, we would not recommend using such an online version of the reconstructed clear-sky radiances as the technical work is not justified seen by the overall neutral impact on forecast scores and fits to independent observations. Despite the pronounced improvements in areas where differences in observed and modelled water vapour amount matters, namely in almost cloud free areas in the Tropics, the overall mean drying effect is not reduced. As the technical work for using solely the bias correction of $\overline{\text{C37}}$ inside the observation error model is rather manageable we could consider using it operationally in the future after running more tests.

Acknowledgements

We thank Niels Bormann and Stephen English for their valuable comments to an earlier version of this manuscript. Katrin Lonitz's work at ECMWF is funded by the EUMETSAT fellowship programme.

References

P. Bauer, A. J. Geer, P. Lopez, and D. Salmond. Direct 4D-Var assimilation of all-sky radiances. Part I: Implementation. *Q.J.R. Meteorol. Soc.*, 136(652):1868–1885, 2010.

R. Buizza, P. Bechtold, M. Bonavita, N. Bormann, A. Bozzo, T. Haiden, R. Hogan, E. Holm, G. Radnoti, D. Richardson, and M. Sleigh. IFS cycle 43r3 brings model and assimilation updates. ECMWF newsletter (152), 2017.

J. R. Eyre. Observation bias correction schemes in data assimilation systems:a theoretical study of some of their properties. *Q.J.R. Meteorol. Soc.*, (142):2284–2291, 2016.

A. J. Geer and P. Bauer. Enhanced use of all-sky microwave observations sensitive to water vapour, cloud and precipitation. *ECMWF Tech. Memo.*, 620, 2010.

A. J. Geer and P. Bauer. Observation errors in all-sky data assimilation. *Q.J.R. Meteorol. Soc.*, 137(661): 2024–2037, 2011.

A. J. Geer, P. Bauer, and P. Lopez. Direct 4D-Var assimilation of all-sky radiances. Part II: Assessment. *Q.J.R. Meteorol. Soc.*, 136(652):1886–1905, 2010.

A. J. Geer, F. Baordo, K. Lonitz, N. Bormann, P. Chambon, S.J. English, M. Kazumori, H. Lawrence, P. Lean, and C. Lupu. The growing impact of satellite observations sensitive to humidity, cloud and precipitation. *Q.J.R. Meteorol. Soc.*, 143:3189–3206, 2017.

N. C. Grody, A. Gruber, and W. C. Shen. Atmospheric water content over the tropical Pacific derived from the Nimbus-6 scanning microwave spectrometer. *Journal of Applied Meteorology*, 19:986–996, 1990.

U. Karstens, C. Simmer, and E. Ruprecht. Remote sensing of cloud liquid water. *Meteorology and Atmospheric Physics*, 54(1):157–171, 1994.

K. Lonitz and A. J. Geer. EUMETSAT/ECMWF Fellowship Programme Research Report: Effect of assimilating microwave imager observations in the presence of a model bias in marine stratocumulus. Technical Report 44, ECMWF, 2017.

G. W. Petty. *A first course in atmospheric radiation*. Sundog Publishing, Madison, Wisconsin, 2nd edition, 2006.